Check for updates

Original Research Article

Protective Effects of *Althaea officinalis* L. Against Cyclophosphamide-induced Immunosuppression and Bone Marrow/Spleen Injuries in Rats

Pharmacognosy Magazine
22(4) 1356–1370, 2026
© The Author(s) 2025
Article reuse guidelines:
in.sagepub.com/journals-permissions-india
DOI: 10.1177/09731296251396325
journals.sagepub.com/home/phm
Sage

Min Sun[1], Shengju Wu[2], Guozhen Yi[3] and Li Yu[4]

Abstract

Background: Chemotherapy targets rapidly dividing cells, impacting HSCs and hematopoiesis.
Objectives: We evaluated the protective impacts of *Althaea officinalis* L. extract (AOE) against cyclophosphamide (CP)-related immunosuppression and damage to the spleen and bone marrow (BM) in rats.
Materials and Methods: Sixty Wistar rats were assigned to six groups: a sham group receiving saline, a CP group receiving 100 mg/kg CP for 10 days, co-treatment groups receiving CP and AOE at doses of 250, 500, and 750 mg/kg for 35 days, and an AOE group receiving 750 mg/kg for 35 days. On day 36, rats were euthanized, and blood specimens were collected. Serum antioxidant enzyme levels (catalase, superoxide dismutase, glutathione peroxidase), nitric oxide levels, total antioxidant levels, and lipid peroxidation in spleen tissues were evaluated. Hematological parameters and cytokine levels were evaluated, alongside the expression of pro-apoptotic-related genes (Bcl-2, caspase-3, Bax, p53).
Results: AOE treatment significantly reduced IL-6 and IL-1β levels and increased IL-10 levels in a dose-dependent manner (p <0.05). Furthermore, AOE significantly improved antioxidant enzyme activities, increased hematological parameters and decreased NO levels (p <0.05). AOE treatment markedly attenuated pro-apoptotic gene expression and enhanced Bcl-2 levels (p <0.05). Immunohistochemical analysis confirmed a significant reduction in p53-positive cells in AOE-treated groups (p <0.05).
Conclusion: AOE enhances hematopoiesis by promoting hematopoietic growth factor production and suppressing inflammatory cytokines, which aids in the proliferation and differentiation of blood cell lineages while reducing apoptosis triggered by CP. The extract's antioxidant, anti-inflammatory, and anti-apoptotic properties effectively counteract CP's harmful effects on bone marrow and spleen tissues.

Keywords

Althaea officinalis L., spleen, cyclophosphamide, bone marrow, immunosuppression

Received 05 April 2025; **revised** 04 July 2025; **accepted** 18 August 2025

Introduction

Chemotherapy is specifically created to target rapidly dividing cells, like cancer cells, the gastrointestinal tract, hair follicles, and hematopoietic stem cells (HSCs), in the bone marrow (BM). HSCs, which undergo frequent cell division, are susceptible to changes in their microenvironment and can enter a dormant state (G_0 phase) in response to chemotherapy or radiotherapy (Chhabra et al., 2016). However, when HSCs in the BM are damaged, their capacity to replicate and differentiate into various blood cells is compromised. This can result in anemia, thrombocytopenia, and neutropenia, which are direct consequences of acute suppression in HSC proliferation. Research indicates that preventing or mitigating BM suppression improves the quality of life and survival

[1]Department of Laboratory, Qinghai Provincial Hospital of Traditional Chinese Medicine, Xining, Qinghai, China
[2]Department of Pulmonary Diseases, Qinghai Provincial Hospital of Traditional Chinese Medicine, Xining, Qinghai, China
[3]Department of Laboratory, Qinghai Province Hainan Tibetan Autonomous Prefecture People's Hospital, Gonghe, Hainan, China
[4]Department of Laboratory, Chengfei Hospital, Sichuan, Chengdu, China
Corresponding author:
Shengju Wu, Department of Pulmonary Diseases, Qinghai Provincial Hospital of Traditional Chinese Medicine, 338 Qiyi Rd, Chengzhong, Xining, Qinghai 810000, China.
E-mails: shengju_20250106@sina.com; ygz996199@sina.com

Creative Commons Non Commercial CC BY-NC: This article is distributed under the terms of the Creative Commons Attribution-NonCommercial 4.0 License (http://www.creativecommons.org/licenses/by-nc/4.0/) which permits non-Commercial use, reproduction and distribution of the work without further permission provided the original work is attributed as specified on the SAGE and Open Access pages (https://us.sagepub.com/en-us/nam/open-access-at-sage).

rates of individuals undergoing chemotherapy and significantly enhances the effectiveness of chemotherapy and radiotherapy as treatment strategies (Sailor et al., 2022). The impact of chemotherapy drugs on HSCs involves triggering cellular senescence and apoptosis pathways, such as the p38/mitogen-activated protein kinase (MAPK) and p53/p21 pathways (Chen et al., 2020). Cyclophosphamide (CP), an alkylating agent, exerts its cytotoxic effects by creating covalent bonds with DNA, causing DNA cross-linking and strand breakage. It is initially a prodrug that undergoes conversion in the liver through the cytochrome P450 system, resulting in the formation of its active metabolite, 4-hydroxycyclophosphamide. This metabolite further breaks down, generating phosphoramide mustard, the primary cytotoxic compound, and acrolein, responsible for certain toxic effects of the drug (Muñiz et al., 2022). CP possesses immunosuppressive properties and finds application in treating various cancer types, as well as autoimmune diseases, such as lupus and rheumatoid arthritis. The drug affects iron metabolism, inhibits DNA replication in HSCs, initiates reactive oxygen species (ROS)-associated apoptosis by activating the intrinsic mitochondria-associated apoptotic pathway in HSCs, directly impacts platelets (PLTs) with cytotoxic effects, thereby hindering hematopoiesis, and causes damage to the BM (Chen et al., 2024). In the current clinical practice, one approach to diagnose and manage BM damage involves the use of hematopoietic growth factors (HGFs), specifically colony-stimulating factors for granulocyte-macrophage (GM-CSF) and granulocytes (G-CSF). HGFs provide the advantage of enabling the administration of high-dose chemotherapy while minimizing side effects (Rees et al., 2022). Research indicates that HGFs are effective in preventing chemotherapy-induced leucopenia/neutropenia. Some plants contain antioxidant compounds and other beneficial substances that promote bone healing and support the hematopoietic cycle. These plants decrease the adverse impacts of chemotherapy agents and increase the chemotherapy anti-cancer effects by strengthening the body's resilience against high-dose treatment (Kang et al., 2022; Xu et al., 2022).

Althaea officinalis L., belonging to the Malvaceae family, is highly distributed around the globe but originates from Northern Africa, Eastern Europe, and Asia. It thrives in both high- and moderate-humidity areas, displaying pinkish-white flowers between July and September (Xue et al., 2023). The *Althaea officinalis* L. extract (AOE) consists of polyphenols (isoquercitrin, p-coumaric acid, caffeic acid, hypolaetin-8-glucoside, kaempferol, daidzein, genistein, scopoletin, quercetin, rutin, asparagine, and catechin), tannins, phytosterols, and coumarins (Farhat et al., 2022). In modern medicine, AOE and its active constituents can treat cardiovascular diseases, exert anti-microbial impacts on respiratory tract infections, prevent urolithiasis, and display anti-estrogenic and immunomodulatory properties. *In vitro* studies have indicated that AOE exhibits anti-proliferative activity by suppressing the growth of various cancer cell lines, including breast (AMJ13), lung (A549), and prostate (PC-3; Wang et al., 2023). The components in this plant, such as daidzein, p-coumaric acid, genistein, kaempferol, and quercetin, act via various signaling pathways, including MEK-ERK, AMPK/p53 PI3K/Akt/mTOR, and PI3K-Akt/PKB, while also displaying anti-inflammatory and antioxidant effects. These components have demonstrated the ability to inhibit the growth of brain, lung, colon, breast, and skin tumors in both *in vivo* and *in vitro* models (Izzo et al., 2020; Özdemir & Turan, 2023).

We assessed the effects of AOE on immunosuppression and damage caused by CP on the spleen and BM. The immunomodulatory effects of AOE were evaluated by assessing biochemical, hematological, antioxidant, and anti-apoptotic properties.

Materials and Methods

Althaea officinalis L. Extract (AOE) Preparation

To extract the AOE, the process involved grinding 3,000 g of dried AOE into a powder by a soil grinder. The obtained powder underwent mixing with distilled water and ethanol (30:70 v:v), followed by incubating in the dark at 40°C for 72 h. Following the incubation period, its filtration was done using a No. 42 Millipore paper filter (catalog number: 1442-125, USA), followed by concentrating with a Buchi evaporator (9230; Switzerland). The AOE final yield was 8.3% (250 g), which was then kept at −4°C (Wang et al., 2023).

Experimental Design, Animals, and Grouping

A total of 60 male Wistar rats (180 ± 20 g) aged 7 weeks, purchased from the Tianjin Xinrui Procedures for Laboratory Animal Center. Animals were randomly assigned to 6 groups of 10 rats. They were housed in a controlled environment with a 12-h light/12-h darkness cycle. The temperature and humidity of the facility were kept at 25°C ± 2°C and 45% ± 5%, respectively. Animals received standard laboratory pellets for their diet and clean tap water. The nutritional value of rat pellets used in this study for feeding includes 20%–25% protein, 50%–60% carbohydrates, and 5%–10% fat for energy density. Additionally, the pellets provide 15 units of vitamin A, 20 units of vitamin D, 5 units of calcium, and 6 units of phosphorus per gram. The approval was obtained from the ethics committee of the Tianjin Xinrui Procedures for Laboratory Animal Center (approval number: XinRui-DWLL-2025008). Furthermore, the research was done following the internationally accepted instructions for the care and use of laboratory animals, based on the Canadian Council on Animal Care in 1993.

Sixty male Wistar rats were assigned to six groups (n = 10/group), which are as follows:

Group 1: Sham: Animals received 1 cc of normal saline once a day by gavage for 35 days.

Group 2: CP: Rats received 100 mg/kg CP dissolved in 1 cc of normal saline daily via intraperitoneal (i.p.) injection for 10 consecutive days.
Groups 3–5: AOE and CP co-treatment groups (250, 500, and 750 AOE + CP): Animals received 100 mg/kg CP dissolved in 1 cc normal saline per day via i.p. injection for 10 consecutive days treated with 250, 500, and 750 mg/kg AOE (dissolved in 0.5 cc normal saline) by gavage daily for 35 days.
Group 6: AOE treatment group (750 AOE): Animals received 750 mg/kg AOE (dissolved in 0.5 cc normal saline) by gavage daily for 35 days.

Throughout the 35-day experiment, animals received CP every day at 9:00 AM and AOE at 3:00 PM, continuously for 10 days. The dosages and timing of the administrations were meticulously determined, taking into consideration previous studies and initial inquiries, to ensure the treatment's safety and effectiveness. To determine the optimal therapeutic dosage of AOE, a combination of methods was utilized, which included a review of existing literature, preliminary investigations, and the lethal dose 50 (LD_{50}) method. Its primary objective was to detect an effective and safe dose of AOE that effectively impeded tumor growth with no adverse effects or toxicity in animals. The study included monitoring mortality rates to evaluate the rats' survival, and a Kaplan–Meier curve was built. These assessments examined the impact of the treatments on the survival of the rats throughout the study duration (Elazab et al., 2021; Li, 2024; Wang et al., 2023).

Biochemical Analysis

On day 36, the rats underwent a 24-h fasting period, after which they were weighed and euthanized following standard laboratory protocols using xylazine (15 mg/kg, i.p.) and ketamine (80 mg/kg). Blood sampling was done via cardiac puncture and separated into two parts. The former was located in tubes containing anti-coagulant for hematological assessment, while the latter was incubated (37°C/15 min). Serum was separated from this second part through centrifugation at 10,000 *g* for 20 min and used to quantify GM-CSF (catalog no.: DY518), G-CSF (catalog no.: MCS00), interleukin (IL)-1β (catalog no.: MLB00C), IL-6 (catalog no.: M6000B), IL-10 (catalog no.: M1000B), and platelet factor 4 (PF4; catalog no.: DY595). R&D Biosystems kits based on the Quantikine QuicKit enzyme-linked immunosorbent assay (ELISA) were utilized, as instructed. The final mixture's absorbance was assessed at 450 nm by an ELISA reader (Spectronic 20; Milton Roy Co., Spain; Lotfi et al., 2020).

Blood Assessment

The blood specimens, which contained the anti-coagulant agent ethylenediaminetetraacetic acid (EDTA), were moved to hematology auto-analyzer devices (Sysmex XW™-100, USA) in order to measure the levels of PLTs, red blood cells (RBCs), and white blood cells (WBCs; Emerson et al., 2025).

Oxidative Stress Evaluation

Nitric Oxide (NO) Assay

Serum NO concentrations were measured by utilizing a commercial kit provided by ZellBio (ZellBio GmbH, catalog no: ZX-44107-96, Germany). The instructions provided by the manufacturer were followed accordingly. Finally, a UV-visible spectrophotometer (model no. Statfax 100, USA) measured the final mixture's absorbance at 540–570 nm (Li, 2024; Wei et al., 2020).

Ferric Reducing Antioxidant Power (FRAP) Assay

Spleen tissue homogenate was prepared by first excising the spleens from the experimental rats under sterile conditions. The spleens were immediately rinsed in cold phosphate-buffered saline (PBS) to remove any residual blood and contaminants. Following this, the tissues were finely minced using sterile scissors and transferred into a pre-chilled homogenization buffer. The minced tissue was then homogenized using a tissue homogenizer at a controlled speed to achieve a uniform suspension. The resulting homogenate was centrifuged at 4°C for 15 min at 10,000 rpm to separate the cellular debris. The supernatant, containing soluble proteins and other biomolecules, was carefully collected and stored at −80°C for subsequent analyses. The FRAP method measured the total antioxidant capacity level. In this method, Fe(III)-2,4,6-Tripyridyl-*S*-triazine (TPTZ) was reduced to Fe(II)-TPTZ by antioxidant compounds. Initially, after the preparation of a working FRAP solution, the final mixture underwent incubation (37°C/15 min). Subsequently, spleen tissue homogenate (150 µL) was combined with the working FRAP mixture (100 µL). The mixture underwent centrifugation at 12,000 g for 15 min and was re-incubated (37°C/15 min). The final supernatant's absorbance was evaluated by a UV-visible spectrophotometer at 593 nm (model no. Statfax 100, USA) against a standard curve of $FeSO_4$, ranging from 0 to 1,000 µM (Wei et al., 2020; Zhou et al., 2024).

Lipid Peroxidation (LPO) Concentrations

The LPO levels in spleen tissue were evaluated by reacting it with thiobarbituric acid (TBA) and malondialdehyde (MDA). In this method, spleen tissue homogenate was prepared using a cold PBS solution, including EDTA, using an ultrasonic homogenizer on frozen tissue. The obtained supernatant was then kept at −70°C. Next, the spleen tissue supernatant (50 µL) was combined with phosphoric acid (1 M; 50 µL), TBA (50 µL), and butylated hydroxytoluene (2 µL) in test tubes. The mixture underwent incubation at 60°C for 1 h. Then it was subjected to centrifugation (12,000 g/5 min), and the supernatant's

absorbance was measured at 532 nm by a UV-visible spectrophotometer (Statfax 100, USA; Wei et al., 2020).

Spleen Tissue Total Thiol Concentrations

For the measurement of the total thiol concentrations in spleen tissue, a homogenized specimen (100 g) was added to tris-EDTA solution (150 µL) and incubated (25°C/10 min). Subsequently, the mixture's initial absorbance (α) was assessed at 412 nm by a UV-visible spectrophotometer (Statfax 100, USA). Then, the mixture was mixed with 5,5-dithio-bis-(2-nitrobenzoic acid) (DTNB; 15 µL) and incubated (25°C/20 min). The ultimate absorbance (β) was noted at 412 nm. Also, the DTNB blank solution's absorbance (μ) was noted at 412 nm. To determine the tissue thiol concentrations, the following formula was utilized:

Total thiol level (µM) = $(\beta - \alpha - \mu) \times 1.07/6.8$ (Wang et al., 2023).

Serum Activity of Glutathione Peroxidase (GPx), Catalase (CAT), and Superoxide Dismutase (SOD)

The SOD (catalog no.: E-EL-R1424), GPx (catalog no.: E-EL-R2491), and CAT (catalog no.: E-BC-K031-S) activity was assessed by the Elabscience commercial kit (Elabscience Biotechnology Co., USA) following the kit protocol's recommendations. Finally, the mixture's absorbance was noted at 450 nm by a Milton Roy spectrophotometer (Spectronic 20, Milton Roy Co., Spain), reporting as U/mL (Shaldoum et al., 2021).

Real-time Polymerase Chain Reaction (Real-time PCR) Analysis of p53, Bax, B-cell Lymphoma 2 (Bcl-2), and Caspase-3 Genes

RNA Extraction

For RNA extraction, we utilized the Bio Basic Animal Total RNA Purification Kit (Cat no: EZ-10; Bio Basic Inc., Canada) and processed 60 mg each of spleen and femur BM tissues. The tissues were snap-frozen in liquid nitrogen and ground into a fine powder using a mortar and pestle while kept frozen. The powdered tissue was then transferred to a 1.5 mL RNase-free tube, and 600 µL of the provided homogenization buffer was added. The mixture was vortexed thoroughly to ensure complete homogenization. Following this, the homogenate was centrifuged at 12,000 × *g* for 10 min at 4°C, and the supernatant was carefully transferred to a new RNase-free tube without disturbing the pellet. An equal volume of 70% ethanol (600 µL) was added to the supernatant, mixed gently by pipetting, and transferred to the RNA-binding column, which was subsequently centrifuged at 12,000 × *g* for 1 min. The flow-through was discarded, and the column was washed by adding 700 µL of wash buffer, followed by another centrifugation at 12,000 × *g* for 1 min. The flow-through was discarded again, and a second wash was performed with 500 µL of wash buffer. To remove any residual wash buffer, the column was centrifuged at 12,000 × *g* for 2 min. For RNA elution, the column was placed in a new RNase-free tube, and 50 µL of RNase-free water was added directly to the center of the column membrane. After a 1-min incubation at room temperature, the column was centrifuged at 12,000 × *g* for 1 min to elute the RNA, which was then stored at −80°C for long-term preservation. Subsequently, the purity and quality of the extracted RNA from the tissues were evaluated using a NanoDrop spectrophotometer (E = A_{260}/A_{280} and A_{260}/A_{230} nm) from Bio-TeK, USA, and a 2% agarose gel. Finally, the extracted RNA was preserved at −80°C for future use (Shaldoum et al., 2021).

Quantitative Real-time PCR (qRT-PCR) and cDNA Synthesis

cDNA synthesis was conducted using the BioFact™ cDNA synthesis kit, starting with total RNA (1 µg) from spleen and BM, mixed with RNase-free water, random hexamer primer, and SYBR Green I Master Mix, oligo-d (T) for an ultimate volume of 20 µL. The reverse transcription involved heating cycles at 95°C for 2 min, 60°C for 30 s, and then a stop at 74°C for 4 min, with the cDNA kept at −20°C. The Primer Express software was designed to generate primers, and they were validated against the National Center for Biotechnology Information (NCBI) database. For qRT-PCR, a 20 µL reaction included cDNA template, Premix ExTaqII Master Mix, oligonucleotides, and double-distilled water (ddH2O) and analyzed the expression of Bcl-2 and pro-apoptotic genes (p53, caspase-3, and Bax) using the Applied Biosystems StepOne™ Real-Time PCR System. The cycling conditions comprised 42 cycles of denaturation, annealing, and extension, along with a melting curve analysis. β-actin was the housekeeping gene for normalization, with mRNA expression levels calculated via the Ct ($2^{-\Delta\Delta CT}$) method, ultimately determining target mRNA expression levels using the following formula:

$\Delta\Delta CT = [(mCT_{target} - mCT_{reference})$ test specimen − $(mCT_{target} - mCT_{reference})$ control specimen].

Then, the target mRNA expression levels were determined using the formula: target mRNA expression level = $2^{-\Delta\Delta CT}$ (Shaldoum et al., 2021).

Immunohistochemistry (IHC) Assay

The presence of p53-positive cells in spleen and BM tissues was assessed as an indicator of apoptotic differentiation in tumor cells. After washing tumor tissues with PBS, standard processing was done to prepare paraffin blocks. Sections (5 µm) were placed on slides, followed by incubation overnight at 95°C using primary p53 antibodies (Cat no: GAF1355, 1:1,000; R&D Systems, Inc., USA). Following this, the slides underwent incubation (1 h/25°C). Tween-20 was the washing

buffer, and 5% bovine serum albumin blocked remaining antibodies. The slides were treated with 3% H_2O_2 for 20 min at 25°C and then stained with 3,3′-diaminobenzidine (DAB). The slides were counterstained with hematoxylin. A BX61TRF optical microscope (Olympus, Japan), coupled with Image J software, examined the slides at 100×. The percentage of p53-positive cells in relation to the total cell numbers was determined by analyzing 10 random fields of view for each specimen (Feng et al., 2024).

Histopathological Analysis

The spleen tissues and femoral BM underwent fixation in 10% formalin for 72 h, gently rinsed with PBS, dehydrated using progressively higher concentrations of ethanol, followed by clearing with xylene, and embedding in paraffin wax. A LEICA SM2010RV1.2 microtome sliced sections of 5 µm from the paraffin blocks (Germany), and then drying was done in an incubator (37°C). After hematoxylin and eosin (H&E) staining, histological analysis of the slides was performed under a light microscope at ×10 and ×40. A BX61TRF calibrated light microscopy system in conjunction with ImageJ software (Olympus, Japan) captured images (Feng et al., 2024).

Statistical Analysis

The survival rate results were analyzed using the Kaplan–Meier test, and the graphs were generated using GraphPad Inc.'s Prism 8. Data analysis was performed using SPSS 16 software. The Kolmogorov-Smirnov test assessed the data normality ($p > .05$). To compare the mean difference between groups, a one-way analysis of variance (ANOVA) test was conducted ($p < .05$ was regarded as significant). Values are mean ± SD. Additionally, the Newman–Keuls test was applied.

Results

Body Weight (BW), Spleen Weight, and Survival Rate (%)

The analysis of the results concerning the BW and spleen weight parameters showed a significant decrease ($p < .05$) in the rats' spleen and BW in the CP group in comparison to the sham group. AOE administration led to an improvement in appetite and a dose-dependent elevation in the rats' weight. After the study, a significant ($p < .05$) elevation in BW and spleen weight was detected in the AOE-treated groups in comparison to the CP group. Notably, the administration of AOE alone (in the 750 AOE group) caused no significant changes in weight parameters in comparison to the sham group (Figure 1A).

Furthermore, the evaluation of the survival rate (%) during the study indicated that the CP group had the lowest survival rate, with four rats dying during the study in this group. In contrast, no deaths were detected in the sham and 750 AOE groups. Additionally, the 500 and 250 AOE + CP groups had two and three rat deaths, respectively, indicating a dose-dependent therapeutic effect of AOE on the survival rate (%; Figure 1B).

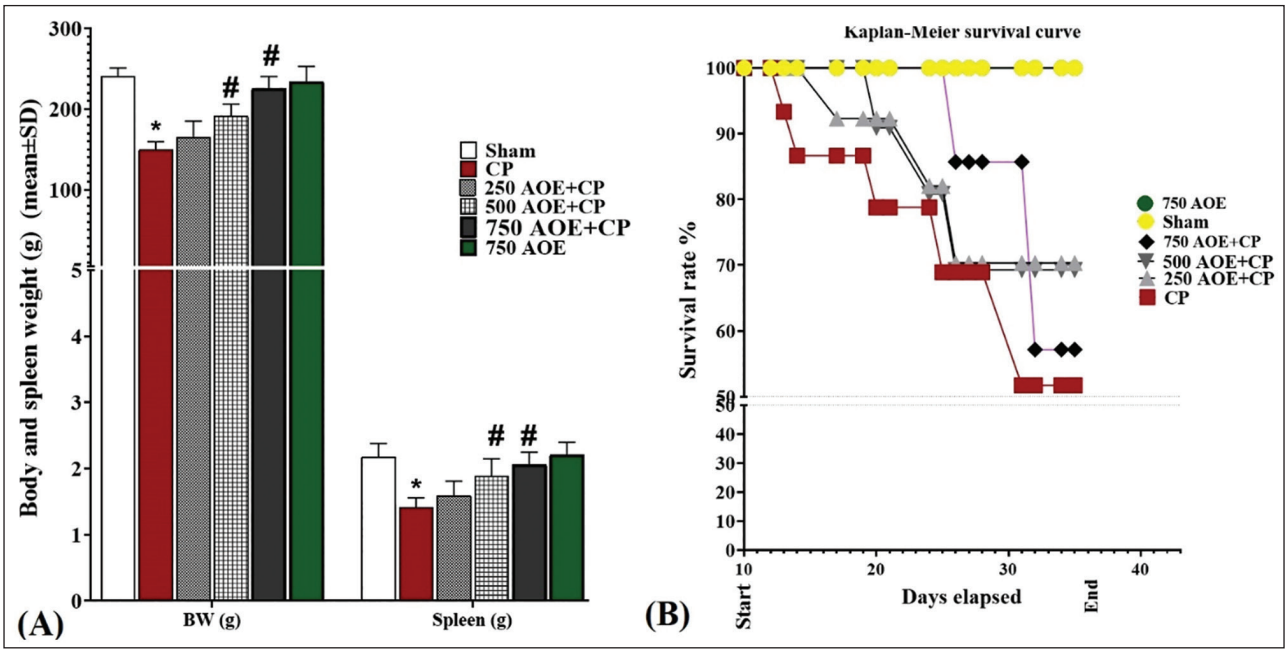


Figure 1. (A) Rats' Body Weight (BW) and Spleen Weight (g). (B) Kaplan–Meier Survival Rate (%) in Different Groups (n = 10/Group; Values are Mean ± SD).

Notes: *($p < .05$) CP versus sham group; #($p < .05$) AOE-treated groups versus CP. AOE: *Althaea officinalis* L. extract; CP: Cyclophosphamide.

IL-6, G-CSF, IL-1β, GM-CSF, IL-10, and PF4 Serum Levels

CP administration resulted in acute systemic inflammation, leading to a notable elevation ($p < .05$) in the serum concentrations of IL-6 and IL-1β, whereas the levels of IL-10 notably decreased ($p < .05$) in comparison to the sham group. Nonetheless, AOE showed a dose-dependent modulation of acute systemic inflammation. In the 250 and 500 AOE + CP groups, the serum IL-6 and IL-1β levels indicated a significant decrease ($p < .05$) in comparison to the CP group, while the serum IL-10 levels notably increased ($p < .05$) in these groups (Figure 2A).

The assessment of serum levels of HSC-stimulating factors (G-CSF and GM-CSF) and PLT inhibitor PF4 in the studied groups showed that CP significantly ($p < .05$) suppressed the G-CSF and GM-CSF synthesis versus the sham group. Conversely, CP significantly ($p < .05$) elevated the serum level of PF4. However, AOE administration stimulated the secretion of G-CSF and GM-CSF in a dose-dependent fashion versus the CP group. Additionally, AOE inhibited the secretion of PF4 from the hematopoietic germ cells and centers. These changes were found to be significant ($p < .05$) in the 500 and 750 AOE + CP groups (Figure 2B).

RBCs, WBCs, and PLTs Count

Based on the results concerning the serum levels of HSC-stimulating factors, it was observed that CP administration led to the suppression of hematopoiesis in comparison to the sham group, which was evident as a significant reduction ($p < .05$) in the counts of RBCs, WBCs, and PLTs. Conversely, AOE administration dose-dependently increased the counts of PLTs, RBCs, and WBCs by stimulating HSC-stimulating factors versus the CP group. This enhancement was found to be significant ($p < .05$) in the 500 and 750 AOE + CP groups (Figure 3).

Serum Activity of SOD, GPx, and CAT and NO Levels

CP significantly increased ($p < .05$) NO concentrations and inhibited ($p < .05$) GPx, SOD, and CAT enzymes in comparison to the sham group. However, AOE, owing to its potent antioxidant capacity, significantly ($p < .05$) decreased the serum NO concentrations and free radicals and significantly ($p < .05$) elevated the GPx, SOD, and CAT activity compared to the CP group. Notably, such alterations were significant ($p < .05$) in the 500 and 750 AOE + CP groups (Figure 4A).

The assessment of parameters related to tissue oxidative stress in the spleen revealed that CP administration significantly ($p < .05$) enhanced MDA and significantly ($p < .05$) decreased tissue antioxidant capacity, as indicated by reduced concentrations of FRAP and thiol, in comparison to the sham group. However, AOE administration dose-dependently reduced MDA levels and increased FRAP and thiol in comparison to the CP group. Such alterations were found to be significant ($p < .05$) in the 500 and 750 AOE + CP groups (Figure 4B).

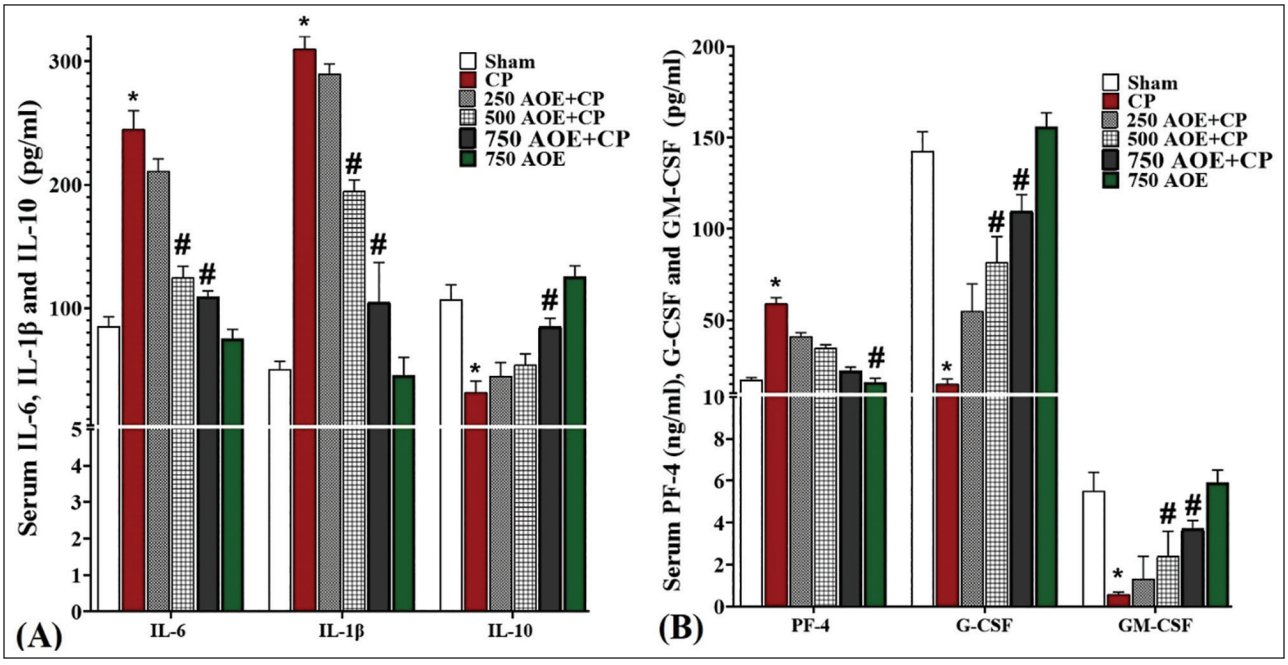


Figure 2. The Mean Serum Levels of (A) IL-1β, IL-6, and IL-10 and (B) PF-4 (ng/mL), G-CSF, and GM-CSF (pg/mL) in Different Groups (n = 10/Group; Values are Means ± SD).

Notes: *($p < .05$) CP versus sham group; #($p < .05$) AOE-treated groups versus CP. AOE: *Althaea officinalis* L. extract; CP: Cyclophosphamide; G-CSF: Colony-stimulating factors granulocytes; GM-CSF: Colony-stimulating factors granulocyte-macrophage; IL: Interleukin.

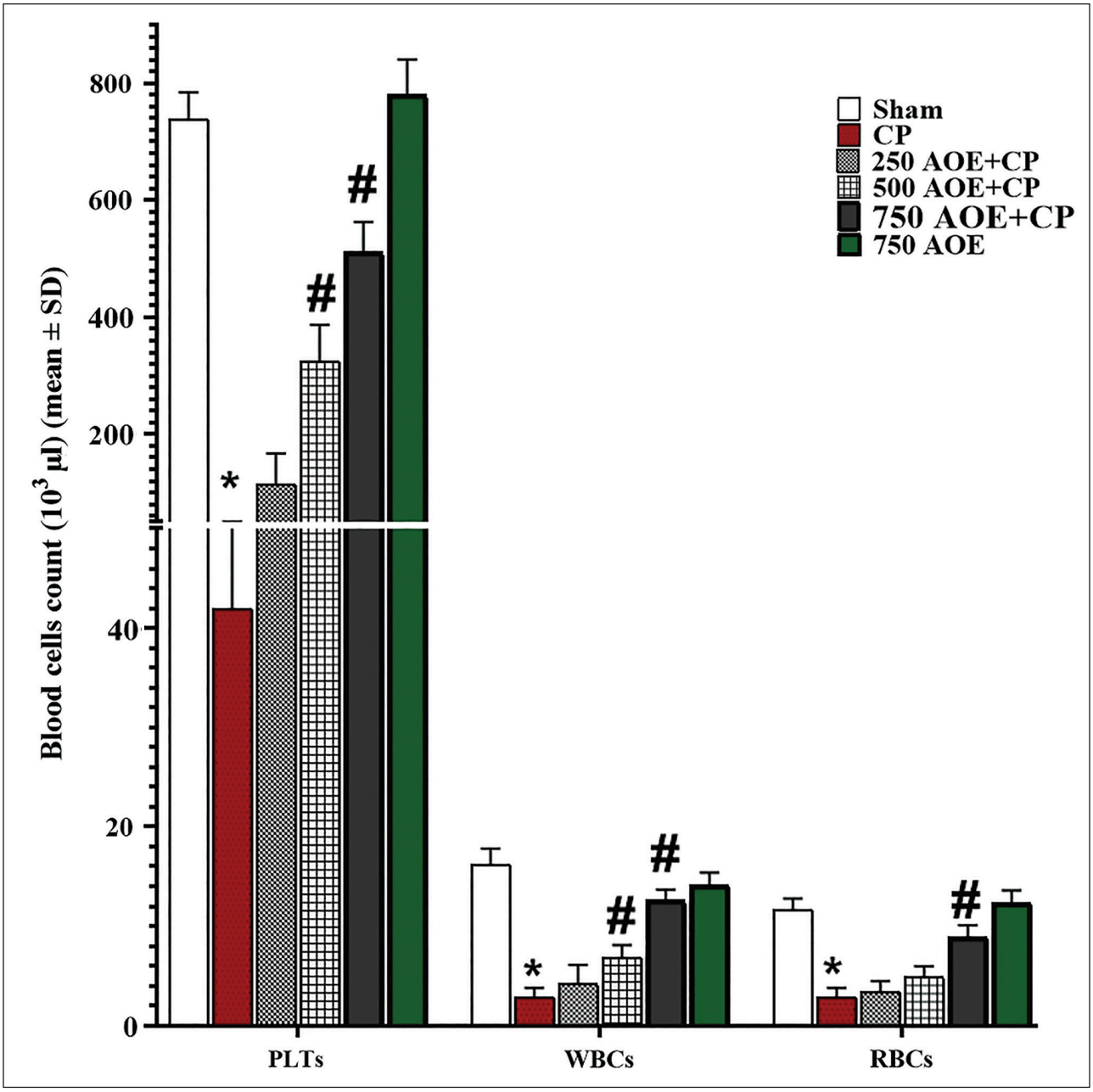


Figure 3. The Mean Counts of Blood Cells (PLT, WBCs, and RBCs) (10^3 µL) in Different Groups (Mean ± SD).

Notes: *($p < .05$) CP versus sham group; #($p < .05$) AOE-treated groups versus CP. AOE: *Althaea officinalis* L. extract; CP: Cyclophosphamide; PLT: Platelets; RBC: Red blood cell; WBC: White blood cell.

Effects of AOE and CP on BM and Spleen and Bcl-2, Bax, Caspase-3, and p53 Expression Levels

CP administration significantly ($p < .05$) upregulated the caspase-3, Bax, and p53 expression levels, while significantly ($p < .05$) downregulating Bcl-2 gene expression in comparison to the sham group. In contrast, AOE dose-dependently inhibited the mitochondrial apoptosis cascade with anti-apoptotic effects. The results revealed that the doses of 500 and 750 AOE (in the 500 and 750 AOE + CP groups) markedly ($p < .05$) attenuated the caspase-3, p53, and Bax expression levels, while markedly ($p < .05$) upregulating the expression of Bcl-2 in both BM and spleen tissues in comparison to the CP group. This indicates the protective effects of AOE in inhibiting pro-apoptotic genes and promoting anti-apoptotic gene expression in these tissues (Table 1, Figures 5 and 6).

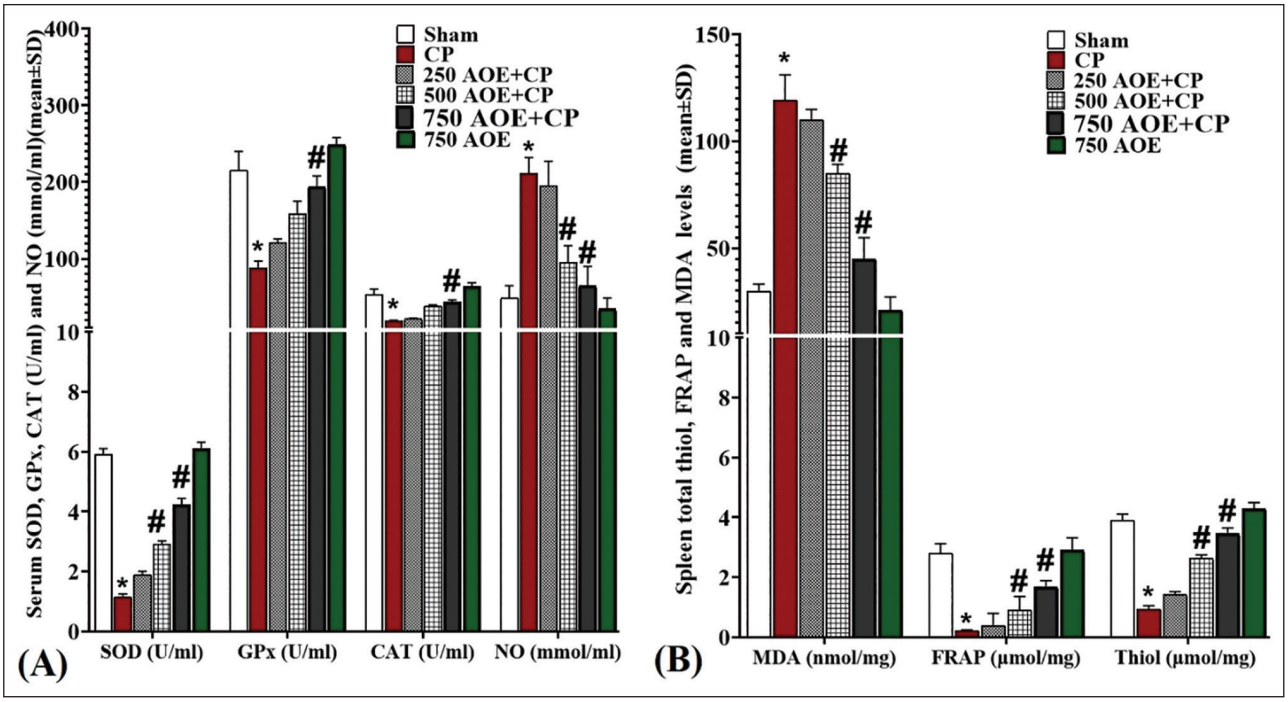


Figure 4. Assessment of Serum and Tissue Antioxidant Status in Different Groups (n = 10/Group; Values are Means ± SD).

Notes: (A) Serum activity of CAT, SOD, and GPx (U/mL). (B) Spleen tissue FRAP (μmol/mg protein), MDA (nmol/mg protein), and total thiol (μmol/mg protein) levels. *($p < .05$) CP versus sham group; #($p < .05$) AOE-treated groups versus CP. AOE: *Althaea officinalis* L. extract; CAT: Catalase; CP: Cyclophosphamide; FRAP: Ferric reducing antioxidant power; GPx: Glutathione peroxidase; MDA: Malondialdehyde; SOD: Superoxide dismutase.

Table 1. Primer Sequences.

Gene	Sequences (5′-3′)
B-cell lymphoma 2 (Bcl-2)	F: ATCGCTCTGTGGATGAC
	R: CAGCCAGCAGAAATCAAACA
Caspase-3	F: GTGGAACTGACGATGATATGG
	R: GCAAAGTGACTGGATGAACC
p53	F: AGAGACCGCCGTACAGAAGA
	R: GCATGGGCATCCTTTAACTC
Bax	F: GCTACAGGGTTTCATCCA
	R: ACATCAGCAATCATCCTCT
β-actin	F: GGCACCACACCTTCTACAATG
	R: GGGGTGTTGAAGGTCTCAAAC

IHC Assay Results for p53 Expression

The immunohistochemical evaluation of p53 expression in BM and spleen revealed that CP treatment led to an elevated rate of apoptosis in cells from these tissues. This effect was evident by a significant elevation ($p < .05$) in the count of p53-positive cells versus the sham group. However, AOE, known for its anti-apoptotic properties, resulted in a dose-dependent reduction of p53-positive cells versus the CP group. Specifically, a significant reduction ($p < .05$) in p53-positive cells was detected in the 500 and 750 AOE + CP groups (Figure 7).

Histopathology Findings

CP treatment resulted in a decrease in cell density within the BM, leading to an increase in fibrous tissue synthesis within the marrow space. This alteration caused an expansion of fat tissue at the expense of hematopoietic tissue. Histopathological examination of the BM tissue revealed degeneration of the hematopoietic parenchyma, which was replaced by interstitial connective tissue. However, administration of AOE dose-dependently increased the presence of hematopoietic parenchyma tissue while significantly reducing fat tissue and interstitial connective tissue. The normal arrangement of

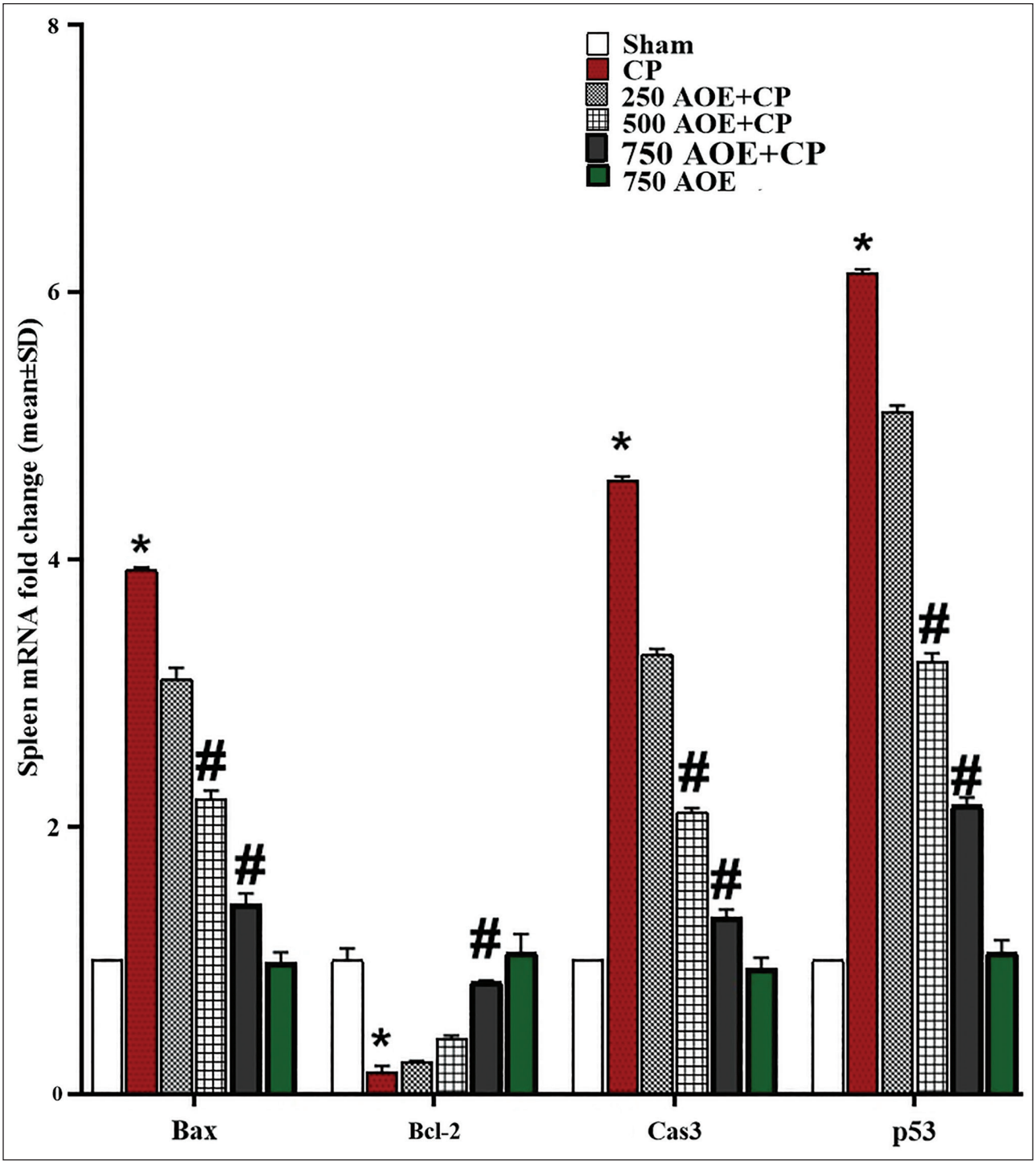


Figure 5. Expression of Caspase-3 (Cas-3), p53, Bax, and B-cell Lymphoma 2 (Bcl-2; Mean ± SD) in Spleen Tissue of Different Groups (n = 10/Group; Values are Means ± SD).

Notes: *($p < .05$) CP versus sham group; #($p < .05$) AOE-treated groups versus CP. AOE: *Althaea officinalis* L. extract; CP: Cyclophosphamide.

hematopoietic germ cells adjacent to trabeculae and within the BM space was observed (Figure 8).

In the evaluation of spleen tissue, CP-induced disruption of the normal arrangement of white and red pulp was observed, along with noticeable congestion in the splenic sinusoids. Dilation of central arterioles in the white pulp, degeneration of the red pulp, and dissolution of capsular trabeculae were also observed. CP treatment led to lymphocyte

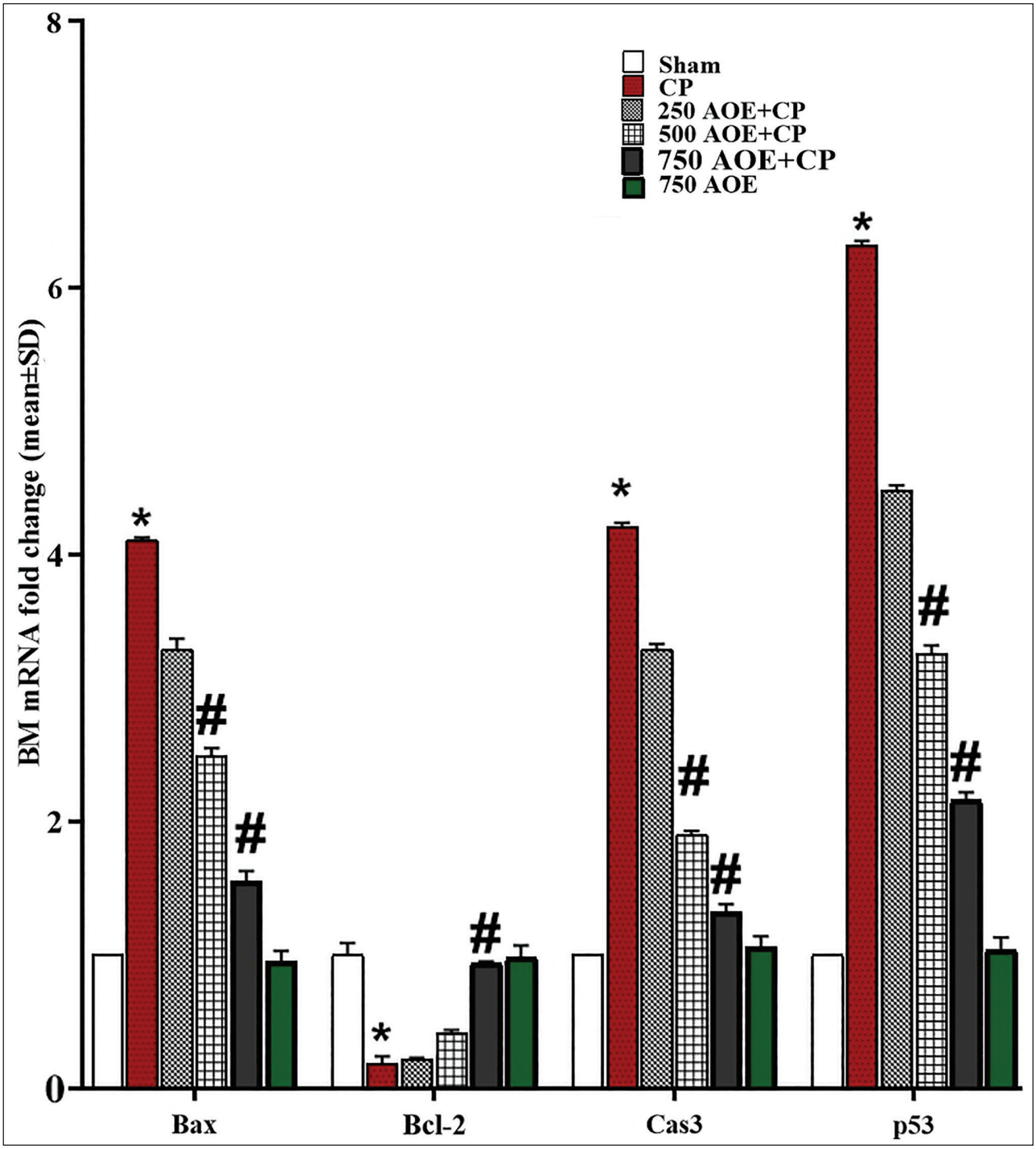


Figure 6. Expression of Caspase-3 (Cas-3), p53, Bax, and B-cell Lymphoma 2 (Bcl-2; Mean ± SD) in Bone Marrow (BM) Tissue of Different Groups (n = 10/Group; Values are Means ± SD).

Notes: *($p < .05$) CP versus sham group; #($p < .05$) AOE-treated groups versus CP. AOE: *Althaea officinalis* L. extract; CP: Cyclophosphamide.

infiltration around the red pulp and sinusoidal cords, with fibrous tissue replacing the pulp parenchyma. In contrast, AOE administration effectively reduced sinusoidal congestion and preserved the diameter of central arterioles in the white pulp. The capsular trabeculae in both white and red pulps appeared in a normal arrangement, and lymphocyte infiltration in the sinusoidal space of the red pulp was not observed (Figure 9).

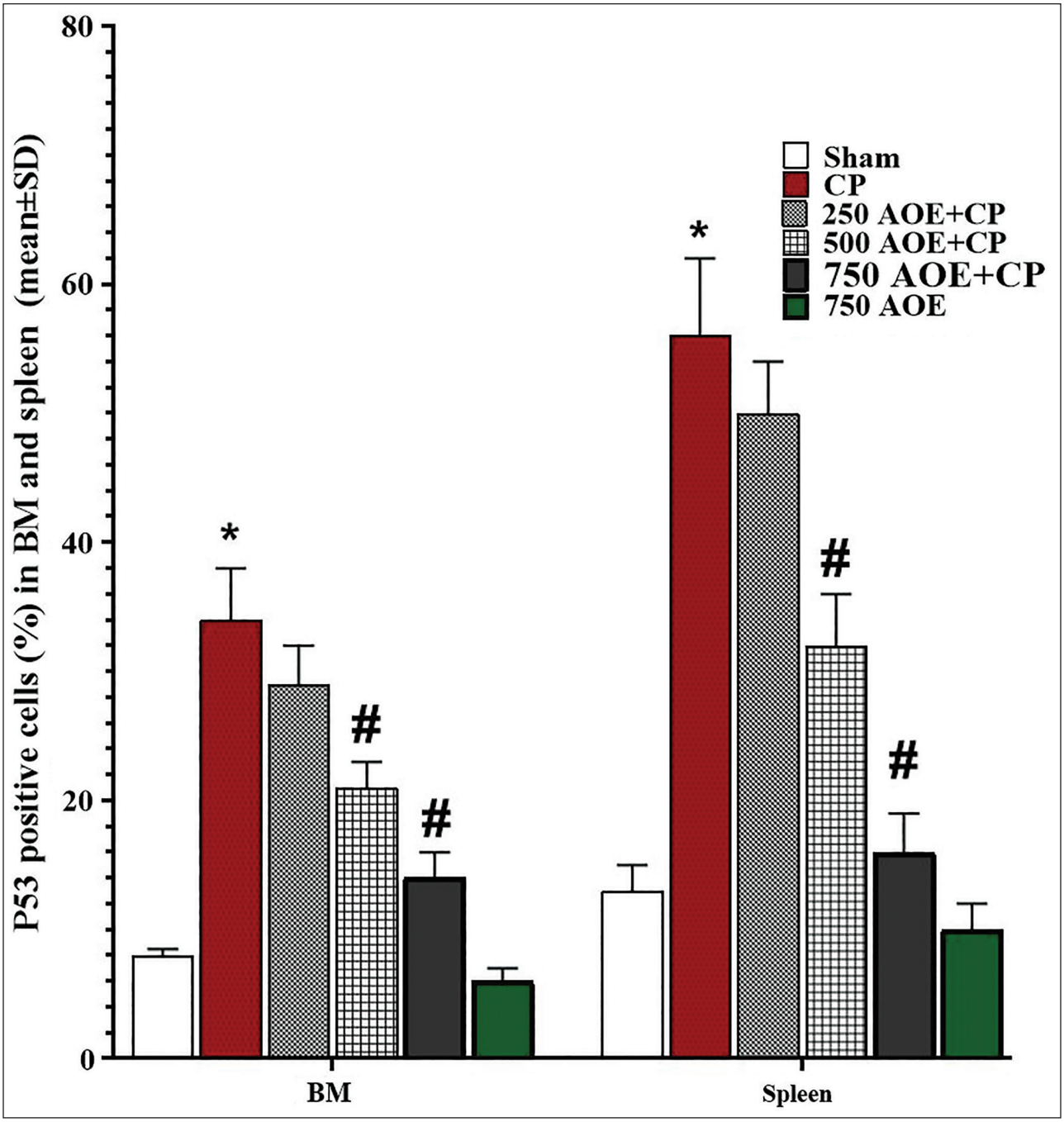


Figure 7 . p53 Positive Cells (%) in Bone Marrow (BM) and Spleen Tissues by Immunohistochemistry (n = 10 Rat/Group, Data are Means ± SD) in Different Groups (n = 10/Group; Values are Means ± SD).

Note: $^{*}(p < .05)$ cyclophosphamide (CP) versus sham group; $^{\#}(p < .05)$ *Althaea officinalis* L. extract (AOE)-treated groups versus CP.

Discussion

The findings of this study demonstrate that AOE possesses antioxidant properties, effectively reducing ROS and LPO in rats exposed to CP. Additionally, AOE exerts anti-apoptotic and anti-inflammatory effects, causing the stimulation of hematopoiesis. Consequently, AOE promotes the proliferation and differentiation of WBCs, RBCs, and PLTs. These beneficial effects highlight the AOE capacity in protecting against chemotherapy-related immunosuppression in cancer patients.

In addition to their anti-proliferative effects on cancer cells through various pathways, chemotherapeutic agents have been observed to inhibit HSCs and elevate blood cell apoptosis by elevating ROS levels. One of the significant CP

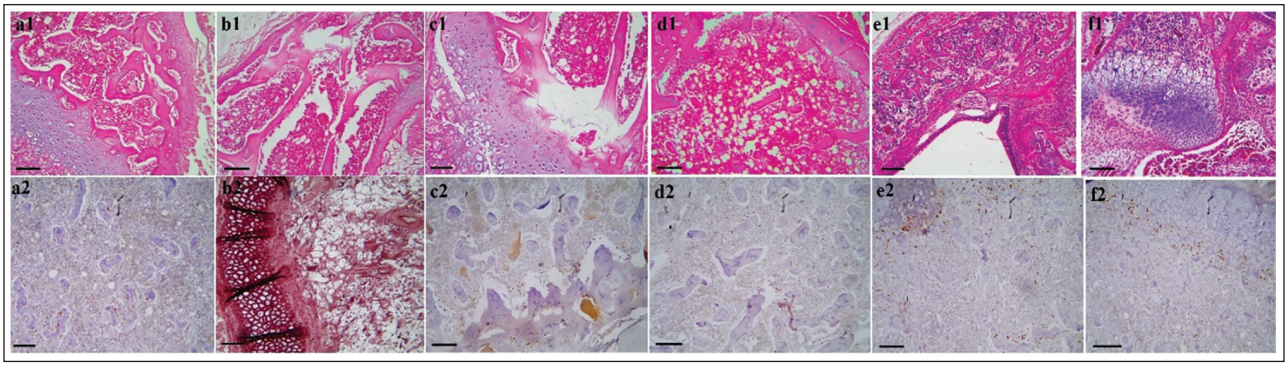


Figure 8. (A) The Bone Marrow (BM) Histopathology in Sham (a1), Cyclophosphamide (CP; b1), 250 *Althaea officinalis* L. Extract (AOE) + CP (c1), 500 AOE + CP (d1), 750 AOE + CP (e1), and 750 AOE (f1) (Hematoxylin and Eosin [H&E], ×10; Scale Bar = 100 µm). (B) Immunohistochemistry (IHC) Staining for p53 in BM Tissue in Sham (a2), CP (b2), 250 AOE + CP (c2), 500 AOE + CP (d2), 750 AOE + CP (e2), and 750 AOE (f2) (H&E, ×10; Scale Bar = 100 µm).

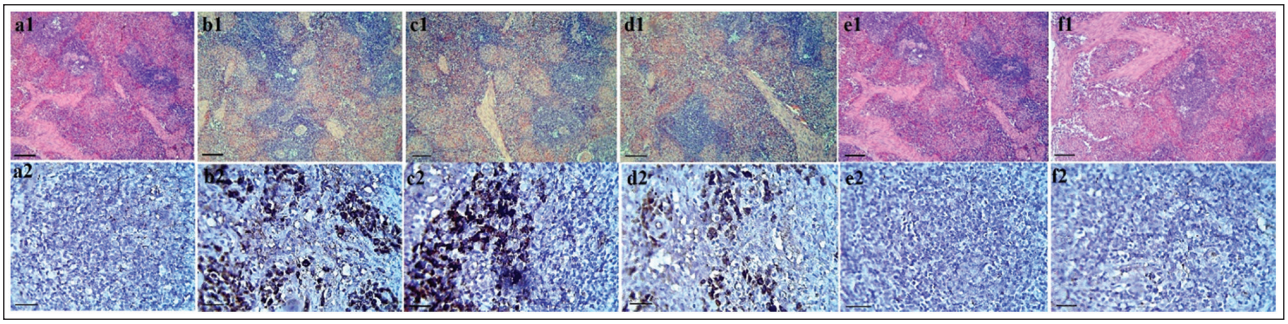


Figure 9. (A) The Spleen Histopathology in Sham (a1), Cyclophosphamide (CP; b1), 250 *Althaea officinalis* L. Extract (AOE) + CP (c1), 500 AOE + CP (d1), 750 AOE + CP (e1), and 750 AOE (f1) (Hematoxylin and Eosin [H&E], ×10; Scale Bar = 100 µm). (B) Immunohistochemistry (IHC) Staining for p53 in Spleen Tissue in Sham (a2), CP (b2), 250 AOE + CP (c2), 500 AOE + CP (d2), 750 AOE + CP (e2), and 750 AOE (f2) (H&E, ×40; Scale Bar = 25 µm).

chemotherapy side effects is BM inhibition, leading to depletion of PLTs, WBCs, and RBCs. This depletion ultimately diminishes the patients' quality of life, reduces the efficacy of chemotherapy, and may even result in patient mortality (Sailor et al., 2022). In tumor-bearing mice, a dosage range of 50−100 mg/kg of CP has been shown to suppress BM, decrease HSCs, and subsequently reduce blood cell counts, leading to thrombocytopenia, anemia, and leukopenia (Elsayed et al., 2022; Fang et al., 2020; Habibi et al., 2020). The metabolism of CP and its metabolites generate ROS, which trigger apoptosis in HSCs through various mitochondrial apoptotic pathways, such as p53, p21, Akt, MAPK, and ataxia telangiectasia mutated (ATM) This ultimately leads to leukopenia, thrombocytopenia, neutropenia, and acute leukemia (Zatalian et al., 2024). Furthermore, ROS induced by CP can cause membrane damage in RBCs and lysis of actin filaments in their matrix. CP primarily suppresses cancer cells by generating ROS and causing injury to their DNA and plasma membrane, triggering apoptosis in cells with a high proliferation rate, such as HSCs. Additionally, studies have demonstrated that a dose-dependent suppression of rat BM occurs with the administration of CP (50 mg/kg), which is attributed to increased NO and MDA levels and also to inhibition of the activity of enzymes like SOD, glutathione-s-transferase, and CAT (Pimenta et al., 2024). The findings of this study indicate that CP can enhance the mitochondrial apoptotic cascade (Bax/Bcl-2-p53-caspase-3 pathway) and promote apoptosis by inducing ROS, inhibiting endogenous antioxidant enzymes (CAT, SOD, and GPx) and increasing LPO (increase MDA levels and decrease FRAP and thiol levels). These effects can lead to the destruction of the membrane of mature blood cells and HSCs, resulting in an elevation in the count of apoptotic cells (p53-positive cells).

AOE was found to enhance the GPx, SOD, and CAT activities, leading to a reduction in free radical levels (NO serum level). This reduction in free radicals increased the antioxidant capacity (FRAP and thiol) and protected cells from LPO. By preserving the integrity of the membrane of parenchymal cells in hematopoietic tissues, AOE inhibited the Bax/Bcl-2-p53-caspase-3 pathway induced by ROS, resulting in a notable decrease in the rate of apoptotic cells (p53 positive). This ultimately helped maintain the tissue structure of the spleen and

BM, and the normal cycle of hematopoiesis/turnover of blood cells was improved, leading to increased proliferation and differentiation of WBCs, RBCs, and PLTs. AOE is rich in polyphenol compounds, with quercetin, genistein, kaempferol, daidzein, and coumarins being the most important ones. According to Čobanová et al. (2020), AOE stimulates the activity of SOD and GPx and increases antioxidant capacity, which leads to a reduction in MDA and NO levels. This ultimately protects hepatocytes against oxidative damage in the indomethacin-related gastric ulcer in rats. In a study by Sutovska et al. (2011), AOE was found to inhibit pro-inflammatory cytokine pathways (resulting in decreased IL-6 and IL-1β secretion) and reduce the inflammatory damage of lung parenchyma and pneumocytes in guinea pigs with ovalbumin-induced airways inflammation (Elhabal et al., 2024). This helped maintain the normal structure and function of the lungs. In another study on an animal model of diazinon-induced hepatotoxicity, AOE protected the structure and function of liver hepatocytes against ROS-induced oxidative damage and apoptosis by enhancing CAT, GPx, and SOD (Morovatisharifabad et al., 2020).

PF4 inhibits colony growth, leading to decreased production of PTLs *in vivo* and ultimately causing thrombocytopenia. Growth factors, including G-CSF and GM-CSF, mediate the survival, differentiation, and proliferation of HSCs through different pathways (He et al., 2022; Meier-Abt et al., 2021). They also elevate the levels of type 1 cytokines (IL-12, IL-6, IL-1β, IL-8, interferon gamma [IFN-γ], and tumor necrosis factor [TNF-α]) while decreasing the concentrations of type 2 cytokines (such as IL-10 and IL-4). G-CSF and GM-CSF not only promote the proliferation of megakaryocytes and leukocytes, such as macrophages, but also enhance their phagocytic potential and increase antibody-related cell-associated cytotoxicity *in vivo* (Zou et al., 2022). Several *in vivo* and *in vitro* studies have demonstrated that CP reduces the GM-CSF and G-CSF systemic levels but increases the IL-8, IL-6, and IL-1β levels. CP increased the secretion of IL-6, IL-10, and IL-1β inflammatory cytokines, along with the stimulation of PF4, which inhibited the secretion of stimulating factors (G-CSF and GM-CSF) of HSCs (Su et al., 2024). Studies show that compounds in AOE can act through different molecular pathways, including IL-6/STAT3, Notch/AKT/mTOR, PI3K/AKT/mTOR, p53/miR-34a/SIRT1, and p53/p21, which control the cell cycle in G2/M and G1 phase and also control the expression of cyclin-dependent kinases (CDKs), especially CDK-2 in parenchymal BM and HSCs (Gao et al., 2024; Wang et al., 2023). AOE can increase the differentiation, survival, and proliferation of blood cells from HSCs by inhibiting the Bax/Bcl-2-p53-caspase-3 pathway and stimulating hematopoietic-stimulating factors, such as G-CSF and GM-CSF. While the findings of this study indicate promising protective effects of AOE against CP-induced immunosuppression and tissue damage, several limitations warrant consideration. The study's duration of 35 days may not fully capture the long-term effects of AOE, and further research is needed to explore its efficacy over extended periods. The use of a single animal model also raises questions about the translational relevance of the results to human patients, as differences in metabolism and physiology may affect outcomes. Furthermore, while the study assessed various biochemical and hematological parameters, the underlying molecular mechanisms by which AOE exerts its protective effects remain to be elucidated.

Conclusion

The crude extract or active compounds of AOE have the potential to safeguard the function and structure of hematopoietic organs against chemotherapy-induced immunosuppression. The extract or compounds exhibited protective effects by stimulating hematopoiesis-stimulating cytokines while inhibiting inflammatory cytokines. This led to the enhanced proliferation and differentiation of blood cell lines, along with the inhibition of the apoptotic cascade mediated by cytochrome c. Moving forward, it is recommended to progress through pre-clinical stages and further investigate additional pathways associated with the effects of AOE extract or active ingredients using diverse human and animal models. Subsequently, considering the potential benefits observed, the use of AOE extract or active ingredients could be explored as an adjunct therapy for individuals undergoing chemotherapy.

Abbreviations

AOE: *Althaea officinalis* L. extract; BM: Bone marrow; CAT: Catalase; CP: Cyclophosphamide; DTNB: 5,5-dithio-bis-(2-nitrobenzoic acid); ELISA: Enzyme-linked immunosorbent assay; FRAP: Ferric reducing antioxidant power; G-CSF: Colony-stimulating factors for granulocytes; GM-CSF: Colony-stimulating factors for granulocyte-macrophage; GPx: Glutathione peroxidase; HGFs: Hematopoietic growth factors; HSCs: Hematopoietic stem cells; MDA: malondialdehyde; SOD: Superoxide dismutase; TBA: Thiobarbituric acid; TPTZ: Tripyridyl-s-triazine; ATM: Ataxia telangiectasia mutated.

Acknowledgments

The authors thank the Qinghai Provincial Hospital of Traditional Chinese Medicine for providing a good research platform.

Declaration of Conflicting Interests

The authors declared no potential conflicts of interest with respect to the research, authorship, and/or publication of this article.

Ethical Approval

The approval was obtained from the ethics committee of the Tianjin Xinrui Procedures for Laboratory Animal Center (approval number: XinRui- DWLL-2025008).

Funding

The authors received no financial support for the research, authorship, and/or publication of this article.

Informed Consent

Not applicable.

ORCID iD

Shengju Wu https://orcid.org/0009-0004-3922-2425

References

Chen, H., Nie, P., Li, J., Wu, Y., Yao, B., Yang, Y., Lash, G. E., & Li, P. (2024). Cyclophosphamide induces ovarian granulosa cell ferroptosis via a mechanism associated with HO-1 and ROS-mediated mitochondrial dysfunction. *Journal of Ovarian Research*, *17*(1), 107. https://doi.org/10.1186/s13048-024-01434-z

Chen, Y., Luo, X., Zou, Z., & Liang, Y. (2020). The role of reactive oxygen species in tumor treatment and its impact on bone marrow hematopoiesis. *Current Drug Targets*, *21*(5), 477–498. https://doi.org/10.2174/1389450120666191021110208

Chhabra, A., Ring, A. M., Weiskopf, K., Schnorr, P. J., Gordon, S., Le, A. C., Kwon, H.-S., Ring, N. G., Volkmer, J., Ho, P. Y., Tseng, S., Weissman, I. L., & Shizuru, J. A. (2016). Hematopoietic stem cell transplantation in immunocompetent hosts without radiation or chemotherapy. *Science Translational Medicine*, *8*(351), 351ra105. https://doi.org/10.1126/scitranslmed.aae0501

Čobanová, K., Váradyová, Z., Grešáková, Ľ., Kucková, K., Mravčáková, D., & Várady, M. (2020). Does herbal and/or zinc dietary supplementation improve the antioxidant and mineral status of lambs with parasite infection? *Antioxidants*, *9*(12), 1172. https://doi.org/10.3390/antiox9121172

Elazab, M. F. A., Younes, A. M., Gaafar, A. Y., Abu-Bryka, A. Z., & Abdel-Daim, M. M. (2021). Immunosuppressive effect of cyclophosphamide in Nile tilapia (Oreochromis niloticus). *Environmental Science and Pollution Research International*, *28*(16), 20784–20793. https://doi.org/10.1007/s11356-020-11893-8

Elhabal, S. F., Abdelaal, N., Saeed Al-Zuhairy, S. A. K., Elrefai, M. F. M., Elsaid Hamdan, A. M., Khalifa, M. M., Hababeh, S., Khasawneh, M. A., Khamis, G. M., Nelson, J., Mohie, P. M., Gad, R. A., Rizk, A., Kabil, S. L., El-Ashery, M. K., Jasti, B. R., Elzohairy, N. A., Elnawawy, T., Hassan, F. E., & El-Nabarawi, M. A. (2024). Green synthesis of zinc oxide nanoparticles from *Althaea officinalis* flower extract coated with chitosan for potential healing effects on diabetic wounds by inhibiting TNF-α and IL-6/IL-1β signaling pathways. *International Journal of Nanomedicine*, *19*, 3045–3070. https://doi.org/10.2147/IJN.S455270

Elsayed, F. F., Elshenawy, W. M., Khalifa, E. M., Rizq, M. R., & Abdelaziz, R. R. (2022). Ameliorative effect of flavocoxid on cyclophosphamide-induced cardio and neurotoxicity via targeting the GM-CSF/NF-κB signaling pathway. *Environmental Science and Pollution Research International*, *29*(46), 69635–69651. https://doi.org/10.1007/s11356-022-20441-5

Emerson, J. F., Wang, H., & Siddiqi, I. N. (2025). Analytical performance of a point-of-care CBC hematology analyzer, including a 5-part differential: A prospective study to evaluate a microfluidic flow cytometry-based analyzer in waived settings. *American Journal of Clinical Pathology*, *163*(4), 531–544. https://doi.org/10.1093/ajcp/aqae149

Fang, H., Xie, X., Liu, P., Rao, Y., Cui, Y., Yang, S., Yu, J., Luo, Y., & Feng, Y. (2020). Ziyuglycoside II alleviates cyclophosphamide-induced leukopenia in mice via regulation of HSPC proliferation and differentiation. *Biomedicine and Pharmacotherapy*, *132*, 110862. https://doi.org/10.1016/j.biopha.2020.110862

Farhat, C., Younes, H., Alyamani, O. A., Mrad, M., Hourani, N., Khalifeh, H., El-Makhour, Y., Dbaibo, G., & Hage-Sleiman, R. (2022). Chemical characterization and *in vitro* biological evaluation of aqueous extract of *Althaea officinalis* L. flower grown in Lebanon. *Journal of Herbal Medicine*, *34*, 100575. https://doi.org/10.1016/j.hermed.2022.100575

Feng, H., Zheng, S., Yang, J., Mao, X., Liu, T., Zhang, Q., & Chen, Y. (2024). Exploring the anti-cancer properties of *Nasturtium officinale* L. via the HOTAIR/miR-124/Notch1 pathway in rat hepatocellular carcinoma: An investigation using biochemical, molecular, immunohistochemical, and histopathological methods. *International Journal of Morphology*, *42*(5), 1361–1372. https://doi.org/10.4067/S0717-95022024000501361

Gao, J., Huang, Y., Song, Y., Huang, X., Zhang, D., & Hou, Z. (2024). Therapeutic effects of *Althaea officinalis* L. and metformin on estradiol-induced polycystic ovary syndrome in rats: Insights into the PI3K/AKT pathway, inflammation, and oxidative stress. *Cell Journal*, *26*(8), 473–486. https://doi.org/10.22074/cellj.2024.2026329.1550

Habibi, E., Shokrzadeh, M., Ahmadi, A., Chabra, A., Naghshvar, F., Haghi-Aminjan, H., & Salehi, F. (2020). Pulmonoprotective action of Zataria multiflora ethanolic extract on cyclophosphamide-induced oxidative lung toxicity in mice. *Chinese Journal of Integrative Medicine*, *26*(10), 754–761. https://doi.org/10.1007/s11655-018-2984-4

He, K., Liu, X., Hoffman, R. D., Shi, R.-Z., Lv, G.-Y., & Gao, J.-L. (2022). G-CSF/GM-CSF-induced hematopoietic dysregulation in the progression of solid tumors. *FEBS Open Bio*, *12*(7), 1268–1285. https://doi.org/10.1002/2211-5463.13445

Izzo, S., Naponelli, V., & Bettuzzi, S. (2020). Flavonoids as epigenetic modulators for prostate cancer prevention. *Nutrients*, *12*(4), 1010. https://doi.org/10.3390/nu12041010

Kang, M., Park, S., Chung, Y., Lim, J.-O., Kang, J. S., & Park, J. H. (2022). Hematopoietic effects of *Angelica gigas* Nakai extract on cyclophosphamide-induced myelosuppression. *Plants*, *11*(24), 3476. https://doi.org/10.3390/plants11243476

Li, J. (2024). Bee pollen and doxorubicin by synergistic effects inhibit the proliferation of breast tumors in 4T1 tumor-bearing BALB/c mice: A biochemical, immunohistochemical, and molecular approach. *Pharmacognosy Magazine*, *20*(1), 159–178. https://doi.org/10.1177/09731296231203809

Lotfi, N., Zhang, G.-X., Esmaeil, N., & Rostami, A. (2020). Evaluation of the effect of GM-CSF blocking on the phenotype and function of human monocytes. *Scientific Reports*, *10*(1), 1567. https://doi.org/10.1038/s41598-020-58131-2

Meier-Abt, F., Wolski, W. E., Tan, G., Kummer, S., Amon, S., Manz, M. G., Aebersold, R., & Theocharides, A. P. A. (2021). Reduced CXCL4/PF4 expression as a driver of increased human hematopoietic stem and progenitor cell proliferation in polycythemia vera. *Blood Cancer Journal*, *11*(2), 31. https://doi.org/10.1038/s41408-021-00423-5

Morovatisharifabad, M., Salehi, E., & Lotfi, Z. (2020). Protective effects of alcoholic extract of *Althaea officinalis* on diazinone-induced liver toxicity in adult male hamsters. *Journal of Applied Biology*, *33*(3), 135–153.

Muñiz, P., Andrés-Zayas, C., Carbonell, D., Chicano, M., Bailén, R., Oarbeascoa, G., Suárez-González, J., Gómez Centurión, I.,

Dorado, N., Gallardo, D., Anguita, J., Kwon, M., Díez-Martín, J. L., Martínez-Laperche, C., & Buño, I. (2022). Association between gene polymorphisms in the cyclophosphamide metabolism pathway with complications after haploidentical hematopoietic stem cell transplantation. *Frontiers in Immunology*, *13*, 1002959. https://doi.org/10.3389/fimmu.2022.1002959

Özdemir, F. A., & Turan, M. (2023). Investigation of antimicrobial and anticancer activity of extracts obtained following UV application to *Althaea officinalis* L. callus cultures. *International Journal of Secondary Metabolite*, *10*(3), 425–436. https://doi.org/10.21448/ijsm.1291929

Pimenta, G. F., Awata, W. M. C., Orlandin, G. G., Silva-Neto, J. A., Assis, V. O., da Costa, R. M., Bruder-Nascimento, T., Tostes, R. C., & Tirapelli, C. R. (2024). Melatonin prevents overproduction of reactive oxygen species and vascular dysfunction induced by cyclophosphamide. *Life Sciences*, *338*, 122361. https://doi.org/10.1016/j.lfs.2023.122361

Rees, M. J., Panigrahi, A., Harrison, S. J., Spencer, A., Khong, T., Gibbs, S., Hocking, J., Grigg, A., & Zantomio, D. (2022). The impact of G-CSF alone vs G-CSF and cyclophosphamide mobilisation on autograft immune cell content in multiple myeloma. *Bone Marrow Transplantation*, *57*(6), 1001–1003. https://doi.org/10.1038/s41409-022-01647-0

Sailor, K. A., Agoranos, G., López-Manzaneda, S., Tada, S., Gillet-Legrand, B., Guerinot, C., Masson, J.-B., Vestergaard, C. L., Bonner, M., Gagnidze, K., Veres, G., Lledo, P.-M., & Cartier, N. (2022). Hematopoietic stem cell transplantation chemotherapy causes microglia senescence and peripheral macrophage engraftment in the brain. *Nature Medicine*, *28*(3), 517–527. https://doi.org/10.1038/s41591-022-01691-9

Shaldoum, F., El-Kott, A. F., Ouda, M. M. A., & Abd-Ella, E. M. (2021). Immunomodulatory effects of bee pollen on doxorubicin-induced bone marrow/spleen immunosuppression in rats. *Journal of Food Biochemistry*, *45*(6), e13747. https://doi.org/10.1111/jfbc.13747

Su, W., Liang, Z., Pan, D., Zhang, L., Zhang, Y., Yuan, T., Gao, X., Su, H., & Zhang, H. (2024). Therapeutic effect of notoginseng saponins before and after fermentation on blood deficiency rats. *Experimental and Therapeutic Medicine*, *27*(4), 143. https://doi.org/10.3892/etm.2024.12431

Sutovska, M., Capek, P., Franova, S., Joskova, M., Sutovsky, J., Marcinek, J., & Kalman, M. (2011). *Antitussive activity of Althaea officinalis* L. polysaccharide rhamnogalacturonan and its changes in guinea pigs with ovalbumine-induced airways inflammation. *Bratislavské lekárske listy, 112*(12), 670-675.

Wang, Z., Jiang, X., Zhang, L., & Chen, H. (2023). Protective effects of *Althaea officinalis* L. extract against N-diethylnitrosamine-induced hepatocellular carcinoma in male Wistar rats through antioxidative, anti-inflammatory, mitochondrial apoptosis and PI3K/Akt/mTOR signaling pathways. *Food Science and Nutrition*, *11*(8), 4756–4772. https://doi.org/10.1002/fsn3.3455

Wei, X., Guan, L., Fan, P., Liu, X., Liu, R., Liu, Y., & Bai, H. (2020). Direct current electric field stimulates nitric oxide production and promotes NO-dependent angiogenesis: Involvement of the PI3K/Akt signaling pathway. *Journal of Vascular Research*, *57*(4), 195–205. https://doi.org/10.1159/000506517

Xu, Y., Zeng, F., Jiang, J., Huo, J., Zhao, C., Yan, Z., & Li, L. (2022). The hematopoietic function of medicinal wine Maoji Jiu revealed in blood deficiency model rats. *Evidence-Based Complementary and Alternative Medicine: eCAM*, *2022*(1), 1025504. https://doi.org/10.1155/2022/1025504

Xue, T., Ruan, K., Tang, Z., Duan, J., & Xu, H. (2023). Isolation, structural properties, and bioactivities of polysaccharides from *Althaea officinalis* Linn.: A review. *International Journal of Biological Macromolecules*, *242*(4), 125098. https://doi.org/10.1016/j.ijbiomac.2023.125098

Zatalian, N., Dalman, A., Afsharian, P., Hezavehei, M., & Gourabi, H. (2024). Metformin protects prepubertal mice ovarian reserve against cyclophosphamide via regulation of the PI3K/Akt/mTOR signaling pathway and Yap-1. *Journal of Ovarian Research*, *17*(1), 251. https://doi.org/10.1186/s13048-024-01572-4

Zhou, C., Qin, X., Wang, J., & Liu, Y. (2024). Anticancer effects of *Vaccinium arctostaphylos* L. through HOTAIR/miR-124/Notch1 axis of hepatocellular carcinoma in rat: A biochemical, molecular, immunohistochemical, and histopathological approaches. *Pharmacognosy Magazine*, *20*(4), 1114–1127. https://doi.org/10.1177/09731296241264620

Zou, J., Zhao, Z., Song, X., Zhang, G., Li, H., Zhang, Q., & Pyykkö, I. (2022). Elevated G-CSF, IL8, and HGF in patients with definite Meniere's disease may indicate the role of NET formation in triggering autoimmunity and autoinflammation. *Scientific Reports*, *12*(1), 16309. https://doi.org/10.1038/s41598-022-20774-8